Numerical simulation studies for the first-light adaptive optics system of the Large Binocular Telescope

Marcel Carbillet*, Armando Riccardi, Simone Esposito

INAF – Osservatorio Astrofisico di Arcetri (OAA), largo E. Fermi 5, 50125 Firenze, Italy

[marcel@arcetri.astro.it | riccardi@arcetri.astro.it | esposito@arcetri.astro.it]

ABSTRACT

We present our latest results concerning the simulation studies performed for the first-light adaptive optics (AO) system of the Large Binocular Telescope (LBT), namely WLBT. After a brief description of the "raw" performance evaluation results, in terms of Strehl ratios attained in the various considered bands (from V to K), we focus on the "scientific" performance that will be obtained when considering the subsequent instrumentation that will benefit from the correction given by the AO system WLBT and the adaptive secondary mirrors LBT 672. In particular, we discuss the performance of the coupling with the instrument LUCIFER, working at near-infrared bands, in terms of signal-to-noise values and limiting magnitudes, and in both the cases of spectroscopy and photometric detection. We also give the encircled energies that are expected in the visible bands, result relevant in one hand for the instrument PEPSI, and in other hand for the "technical viewer" that will be on board the WLBT system itself.

Keywords: Large Binocular Telescope, first-light adaptive optics system, performance evaluation

1. INTRODUCTION

The first-light adaptive optics (AO) system of the Large Binocular Telescope (LBT) is foreseen to operate at the end of 2004. It is a part of the acquisition, guiding and wavefront sensing (AGW) unit of LBT, and it is named WLBT. A complete description of the system is given in Esposito et al.,[3] while the LBT 672 adaptive secondary mirror features are described in Riccardi et al.[6] In this paper we focus on the latest numerical studies we have made in order to evaluate the performance of the whole system.

Those are given first in terms of Strehl ratios in the whole set of bands considered (from V to K), taking into account for the bands R and I to distribute 50% of the light between the wave-front sensor (working between 600 and 900 nm) and the scientific instrument. These "raw" results are given together with the optimal values found for the ensemble of system parameters (sensor configuration, exposure time, number of LBT 672 modes controlled, pyramid modulation) corresponding to each AO guide-star R-magnitude considered.

We have then computed the encircled energies that result from the point-spread functions (PSFs) obtained in each band and for each AO guide-star R-magnitude, showing the great improvement that can be obtained even at short wavelengths (hence relevant to the instrument PEPSI and the "technical viewer" foreseen on board the WLBT system itself).

Finally, we go in more details for the near-infrared performance, i.e. for what concerns the WLBT+LUCIFER performance, both in terms of photometric detection and spectroscopy. For this, we have computed the limiting magnitudes that are reached when considering a given signal-to-noise (SNR), namely 3, a given time exposure (1800 s), and a given spectral resolution.

The paper is hence organized as follows. In Sec. 2 we describe the numerical simulations performed by using the Software Package CAOS, while in Sec. 3 we expose the "raw" performance obtained for the system in terms of Strehl ratios in the whole ensemble of bands considered, together with the resulting optimized WLBT system parameters. Section 4 is then dedicated to the coupling of the WLBT system with the subsequent scientific instrumentation, namely LUCIFER (near-infrared bands), PEPSI (visible bands), and the "technical viewer" intended to work at the sensing wavelength. Finally, we give our conclusions in Sec. 5.

* On move from OAA to Laboratoire Universitaire d'Astrophysique de Nice, UMR 6525, Université de Nice–Sophia Antipolis, Parc Valrose, 06108 Nice Cedex 02, France – Correspondance e-mail: marcel.carbillet@unice.fr

2. SIMULATING THE WLBT SYSTEM WITH CAOS

The "Code for Adaptive Optics Systems"

The simulation tool used for the simulations presented here is the CAOS "system" (where CAOS stands fro Code for Adaptive Optics Systems). It is essentially composed of *Software Packages*, among them the original Software Package CAOS dedicated to AO systems modeling,[1] designed to be used within a graphical programming environment – the CAOS Application Builder[4, 5] where the data flow and the parameters of each module can be set.

The structure of this numerical tool being modular, each physical elementary process of a given simulation is modeled within a specific module – like, in the AO case, the turbulence in each atmospheric layer, the propagation of the light from a source to the observing telescope and through the turbulent layers, the wavefront sensing, the wavefront reconstruction, time-filtering of the resulting deformable mirror commands, the wavefront correction, etc. Taking advantage from the CAOS Application Builder, a simulation can be built putting and connecting together the required occurrences of the desired modules, respecting the only logical constraint given by their formalized type of input/output. Each module comes with an individual GUI in order to set its own physical and numerical parameters, during the design step of a simulation or independently in a later moment. The whole structure of a simulation can be saved as a "project" that can be restored for later modifications and/or parameters upgrading. The IDL code, corresponding to the designed simulation, is written down during the saving of a project, and it can possibly be modified "by hand" in order to be completed with some additional task not provided by strictly using the Software Package CAOS.

More detailed informations about this numerical simulation tool and the already developed associated packages can be found from the dedicated web-site `http://www.arcetri.astro.it/caos`, and from the companion communication within these proceedings.[2]

Simulation procedure followed

Figure 1 shows the simulation procedure followed, within the CAOS Application Builder and using the modules of the Software Package CAOS, for simulating the WLBT system and the resulting PSF morphology for the various wavelength bands and off-axis values considered here.

The output of the module `ATM` simulating the atmosphere (made of two moving turbulent layers) is sent to module `ATA` that mimics the correction due to the deformable mirror (the adaptive secondary mirror LBT 672 in our case) into a "correction" layer (here conjugated to the ground). The resulting corrected wavefront is then computed by the module `GPR` that basically propagates the light between the guide star defined within module `SRC` and the telescope which characteristics are set by using the GUI of `GPR`. The resulting corrected wavefront is then taken into account by module `PYR` that simulates the behavior of the pyramid wavefront sensor, and the resulting signals are then sent to a slope calculator (`SLO`) that compute the slopes corresponding to each subaperture of the pyramid wavefront sensor, before sending the result to the wavefront reconstructor `RCC` that reconstruct the wavefront by using the LBT 672 computed modes. The loop is then closed by a special module (part of the Application Builder) that send the result to previously evoked module `ATA`. During each step of the simulation the resulting PSFs are computed within the occurrences of module `IMG` in the Johnson bands V, R, I, J, H, and K. These PSFs are here calculated with no background nor noise contributions in order to be used latter varying the object magnitude, time-exposures, and noise contributions (see next section). Note that, instead, the on-axis star (occurrence `#003` of module `SRC` in the figure) magnitude is fixed as it is also the AO guide star considered, and the series of system parameters are being varied accordingly in order to find the optimum set of them permitting the best AO correction.

A quite noticeable remark is that each process is simulated as close as possible to the real-life situation. For example the pyramid sensor, in which diffraction effects play a certain role on the performance of the system, is simulated following the following scheme: the electric field in the image plane is masked for each facet of the pyramid, resulting after diffraction computation in the four-pupil image of Fig. 1. The pyramid can also be simulated by simulating the pyramid as a phase mask. Still for the pyramid, we here consider a standard CCD device, but we could also consider an low-light-level CCD, for which the photon noise is not anymore Poisson-like, and an "exotic" dark current component has to be taken into account.

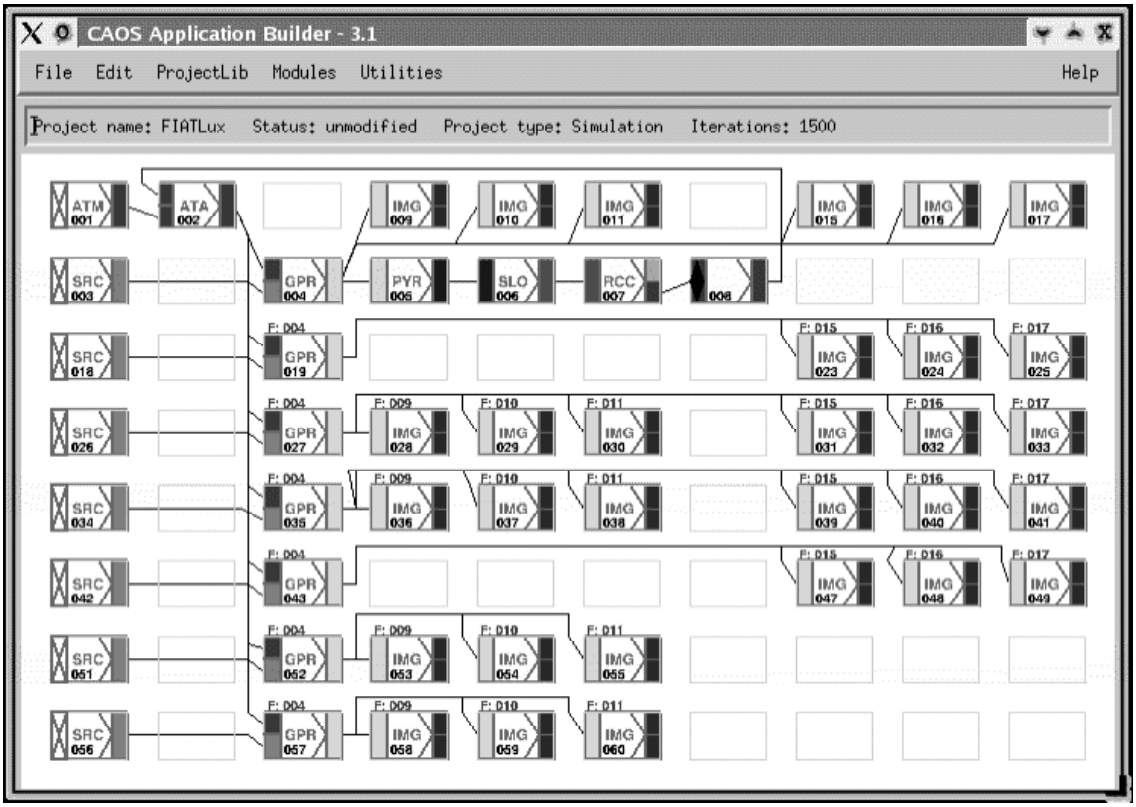

Figure 1. Simulation procedure followed for simulating the WLBT system by means of the CAOS Application Builder and the Software Package CAOS. The different occurrences of module `SRC` correspond to different off-axis values considered for the observed object, while the different occurrences of module `IMG` correspond to the various imaging bands considered (V,R,I,J,H,K) for each of the object off-axis values.

We have designed this typical simulation for the different configurations of the wavefront sensor and ran it for a wide range of parameters defining each consecutive process of the whole simulation, exploring so the hyper-space of parameters as extensively as possible, and finally finding the set of optimum values.

3. WLBT SYSTEM "RAW" PERFORMANCE EVALUATION

The performance of the WLBT system have been evaluated following the procedure exposed in previous section. The main parameters associated with this wide series of simulations are reported in Table 1, but concerning the read-out noise (RON) values corresponding to the CCD adopted, which are reported in Table 2.

The hyper-space of free parameters has been explored by different simulation realizations, and the result in terms of optimized system parameters is given in Table 3.

The final result is given in Fig. 2, in terms of terms of Strehl ratios in the various Johnson bands considered, namely V, R, I, J, H, and K. It has to be noted that while the light is well separated for the near-infrared bands (J,H,K), it has to be splitted between the wavefront sensor (working between 600 and 900 nm – basically band R and a part of band I) and the scientific channel for the visible bands R and I, while for band V the situation is equivalent to the near-infrared wavelength bands. As a consequence, the wavefront sensing more suffers from photon starving in the bands R and I (in addition to the poorer correction from the AO system), and this is directly propagated in the results shown in the figure. We have chosen to split the light as follows for the bands R and I: 50% to the wavefront sensing and 50% to the scientific channel.

Table 1. Main parameters concerning the simulations made for the WLBT performance evaluation.

turbulent atmosphere parameters	
Fried parameter r_0 (at 500 nm)	15 cm
number of turbulent layers	2
ground layer velocity	~8 m/s
ground layer C_N^2 profile relative percentage	70%
high layer velocity	~16.5 m/s
high layer C_N^2 profile relative percentage	30%
wavefront outer-scale $\mathcal{L}_0$	20 m
telescope parameters	
effective diameter	8.22 m
obstruction ratio	0.11%
AO guide star parameters	
spectral type	K5
R-magnitude	8—17
deformable mirror parameters	
type of adaptive mirror	secondary mirror
number of actuators	672
wavefront reconstruction parameters	
number of modes reconstructed	up to 672
time filter type	pure integration
pyramid sensor parameters	
central sensing wavelength	750 nm
bandwidth	300 nm
pyramid simulation method	transmission mask
standard dark current	none
total average transmission	0.41
configurations	10×10, 15×15, 30×30
exposure time [ms]	1, 1.67, 2.5, 5, 10
RON [e^- rms]	see Table 2
point-spread function forming - visible	
imaging bands	V, R, I
off-axis angles [″]	0, 2.5, 5, 10, 15
pixel size [mas]	5
dimension [px]	251×251
point-spread function forming - near-infrared	
imaging bands	J, H, K
off-axis angles [″]	0, 5, 10, 20, 30
pixel size [mas]	15
dimension [px]	251×251

Table 2. Read-out noise values in function of the exposure time and CCD binning.

Exposure time [ms] / CCD binning → pyramid config.	10	5	2.5	1.67	1
1×1 CCD px → 30×30 sub-ap.	4.5	4.5	5.8	8.4	8.4
2×2 CCD px → 15×15 sub-ap.	3.5	4.5	4.5	5.8	8.4
3×3 CCD px → 10×10 sub-ap.	3.5	3.5	2.5	4.5	5.8

Table 3. Performance evaluation optimized parameters.

K5 star R-mag.	pyramid configuration	Δt [ms]	$\Rightarrow$ RON [e^- rms]	number of modes	pyramid mod. [λ/D]
8	30×30	1.00	$\Rightarrow$ 8.4	671	±1
9	30×30	1.00	$\Rightarrow$ 8.4	500	±1
10	30×30	1.00	$\Rightarrow$ 8.4	450	±2
11	30×30	1.67	$\Rightarrow$ 8.4	400	±2
12	15×15	1.67	$\Rightarrow$ 5.8	150	±3
13	15×15	2.50	$\Rightarrow$ 4.5	130	±3
14	15×15	2.50	$\Rightarrow$ 4.5	105	±3
15	10×10	5.00	$\Rightarrow$ 3.5	60	±4
16	10×10	5.00	$\Rightarrow$ 3.5	55	±5
17	10×10	10.00	$\Rightarrow$ 3.5	45	±6

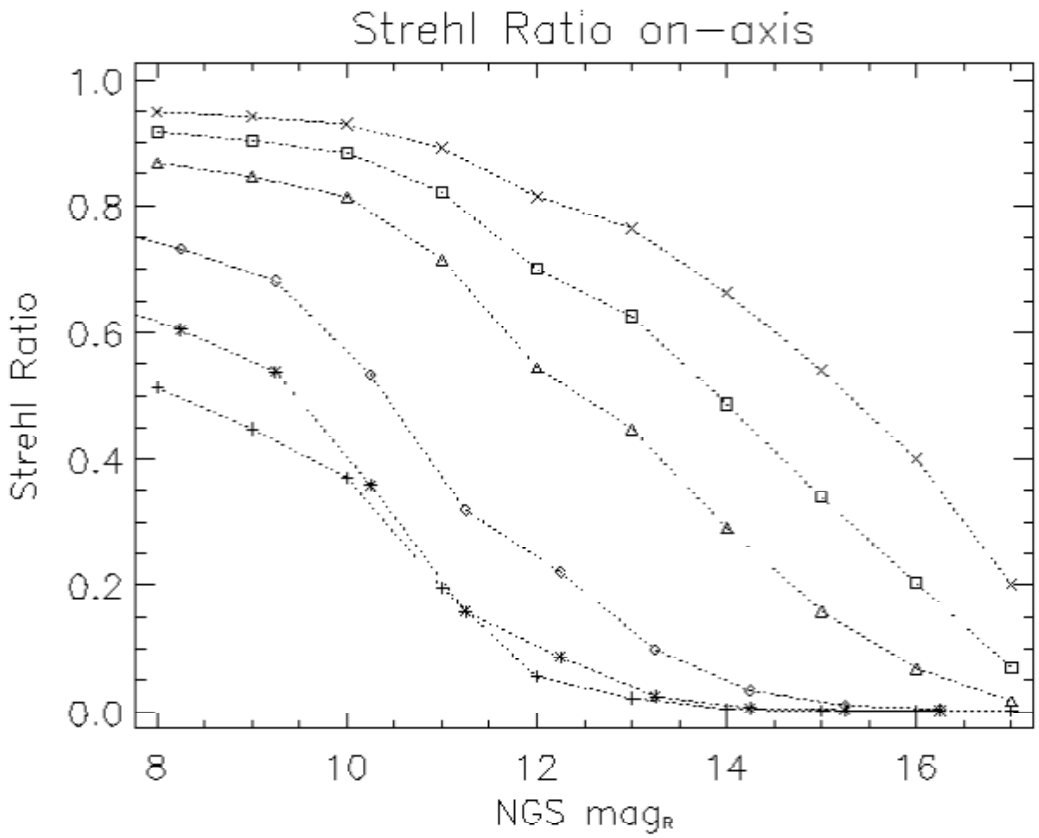

Figure 2. Strehl ratios in bands V (+), R (∗), I (rhombuses), J (triangles), H (squares), and K (×).

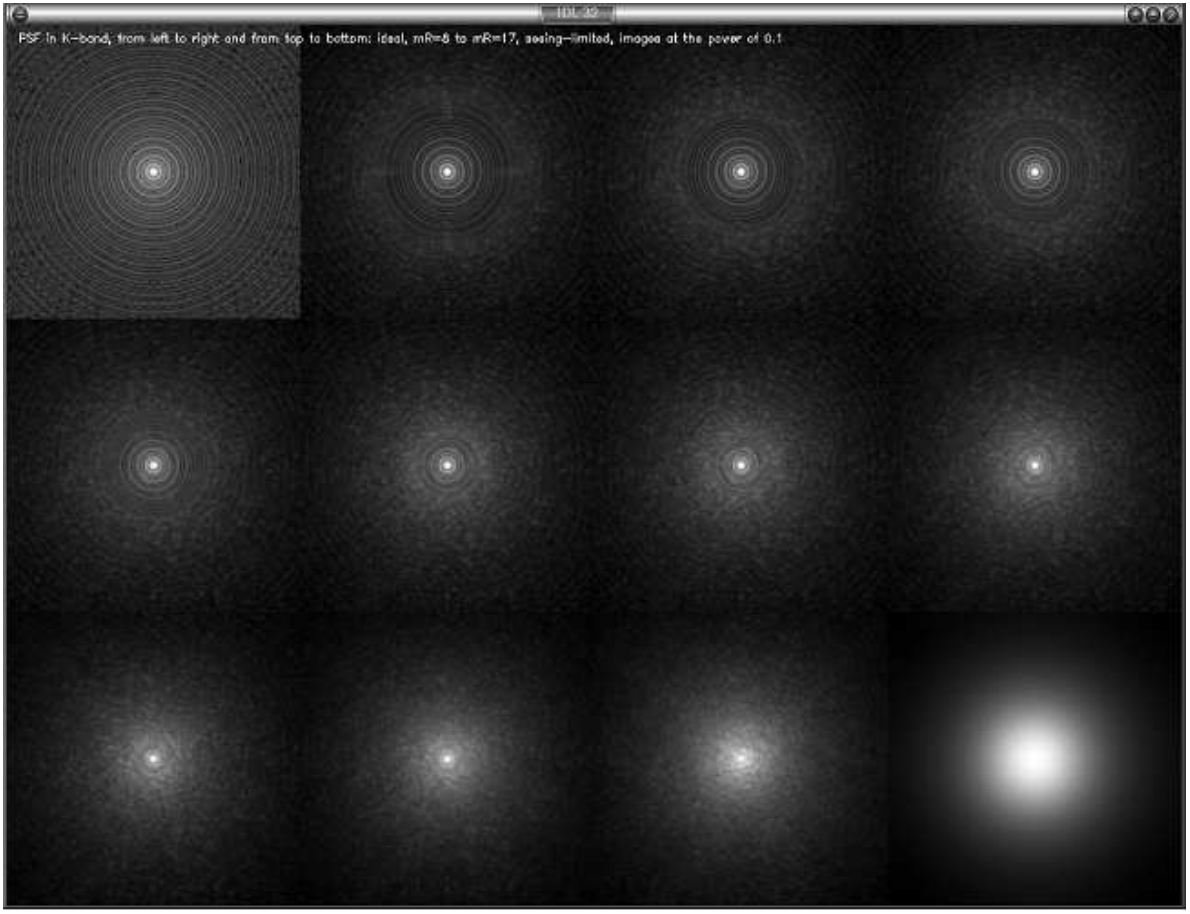

Figure 3. K-band PSFs as a function of the AO guide-star magnitude, represented at the power of 0.1 for sake of clarity. From top to bottom and from left to right: ideal case, R-magnitude cases from 8 to 17, seeing-limited case.

Figure 3 shows the K-band PSFs obtained in function of the R-magnitude of the K5 spectral type AO guide star, together with the diffraction-limited PSF (first figure in the top-left corner) and the seeing-limited one (last figure in the bottom-right corner). The corresponding AO guide star R-magnitudes (spectral type K5) are, from left to right and from top to bottom: 8, 9, 10, 11, 12, 13, 14, 15, 16, and 17.

Note the evolving shape of the resulting PSF. As classically known the Strehl ratio is decreasing with increasing of the AO guide star magnitude, because of the progressive lack of photons. Hence the optimal system parameters are also evolving, as it can be noticed from Table 3: the number of subapertures and the number of corrected modes are decreasing, while the exposure time and the pyramid modulation are increasing. Beside this Strehl ratio evolution the angular resolution is decreasing as well, even if it basically remains close to λ/D for the brightest cases. The global shape of the PSF is also strongly changing, with a speckle-ized halo which level grows with increasing of the AO guide star magnitude.

4. COUPLING WITH THE SUBSEQUENT SCIENTIFIC INSTRUMENTATION

In order to evaluate the actual performance the WLBT system will permit to the subsequent scientific instrumentation, after having completely optimized the AO system parameters for the median atmospheric conditions considered for LBT, and computed the "clean" (no background, no noises contribution) PSF corresponding to the various bands and off-axis values defined in previous section, it is necessary here to vary the object magnitude, background, and noise contributions, corresponding to each band and to a fixed exposure time. The exposure time has been fixed to 30 min (1800 s), and the others relevant parameters are reported in Table 4.

Table 4. Image formation parameters.

band	total average efficiency	Δt [s]	RON [e$^-$]	dark current [e$^-$/s]	sky background
V	0.204	1800	0.5	0.10	21.0 mag./$''^2$
R	0.204	1800	0.5	0.10	20.0 mag./$''^2$
I	0.204	1800	0.5	0.10	19.5 mag./$''^2$
J	0.204	1800	9.0	0.05	15.0 mag./$''^2$
H	0.204	1800	9.0	0.05	12.5 mag./$''^2$
K	0.204	1800	9.0	0.05	13.5 mag./$''^2$

All the subsequent computations, in terms first of the encircled energy, but then in a more interesting way in terms of signal-to-noise and limiting magnitudes obtained, are described hereafter.

Encircled energy

We have computed the encircled energy that results from the previously described PSF simulations. The results obtained, shown in Fig. 4, are clearly depending on the morphology itself of the resulting PSFs in the various bands of interest (visible and near-infrared) and, for the bands in common with the spectral sensing range (600–900 nm), i.e. R and I, on the 50% light distribution chosen (use of a beam-splitter).

From a first evaluation, we remark that, when taking benefit from the high-angular resolution given by the WLBT system, a great gain is achievable in all bands, even the less corrected ones (visible). For example at 50 mas and observing in R-band we have a gain of $\sim$150 going from the seeing-limited (no AO) situation to the case of best correction (AO guide-star of R-magnitude 8), and to $\sim$12.5 for an AO guide-star of R-magnitude 14.

In K-band, we reach a gain from $\sim$50 to $\sim$75 for the AO guide-star from an R-magnitude of 14 to 8, considering again to look at 50 mas. More generally, it is clear from these plots that the gain is impressive especially in the bands I to K from the level of correction given by an median AO guide-star of magnitude 14.

While bands V, R, and I are particularly relevant to the instrument PEPSI and to the "technical viewer" that will be on board the WLBT itself, the near-infrared bands J, H, and K are clearly relevant to the instrument LUCIFER. Next subsection deals with the latter case.

Signal-to-noise ratio and limiting magnitudes – LUCIFER case

In this subsection we go a step forward, evaluating the limiting magnitudes both in photometric detection and spectroscopic modes, starting from a given signal-to-noise (SNR) to be attained and concentrating, for sake of conciseness, on the near-infrared wavelengths. The latter directly corresponds to the instrument LUCIFER, a spectro-imager that will work together with the WLBT system as soon as possible.

Fixing the SNR to be reached, the limiting magnitudes writes:

$$\mathrm{mag_{lim}} = -2.5 \log N/N_0 \tag{1}$$

where N_0 is the number of photons per second for a star of magnitude 0 in the band considered, and:

$$N = \frac{-b + \sqrt{b^2 - 4\,a\,c}}{2\,a}, \text{ with :} \tag{2}$$

$$a = \Delta t^2\,\rho^2, \tag{3}$$

$$b = -\mathrm{SNR}^2\,\Delta t\,\rho,$$

$$c = -n_{\mathrm{px}}\left(\left(N_{\mathrm{bg}} + N_{\mathrm{d}}\right)\Delta t + {\sigma_{\mathrm{e}}}^2\right)\,\mathrm{SNR}^2,$$

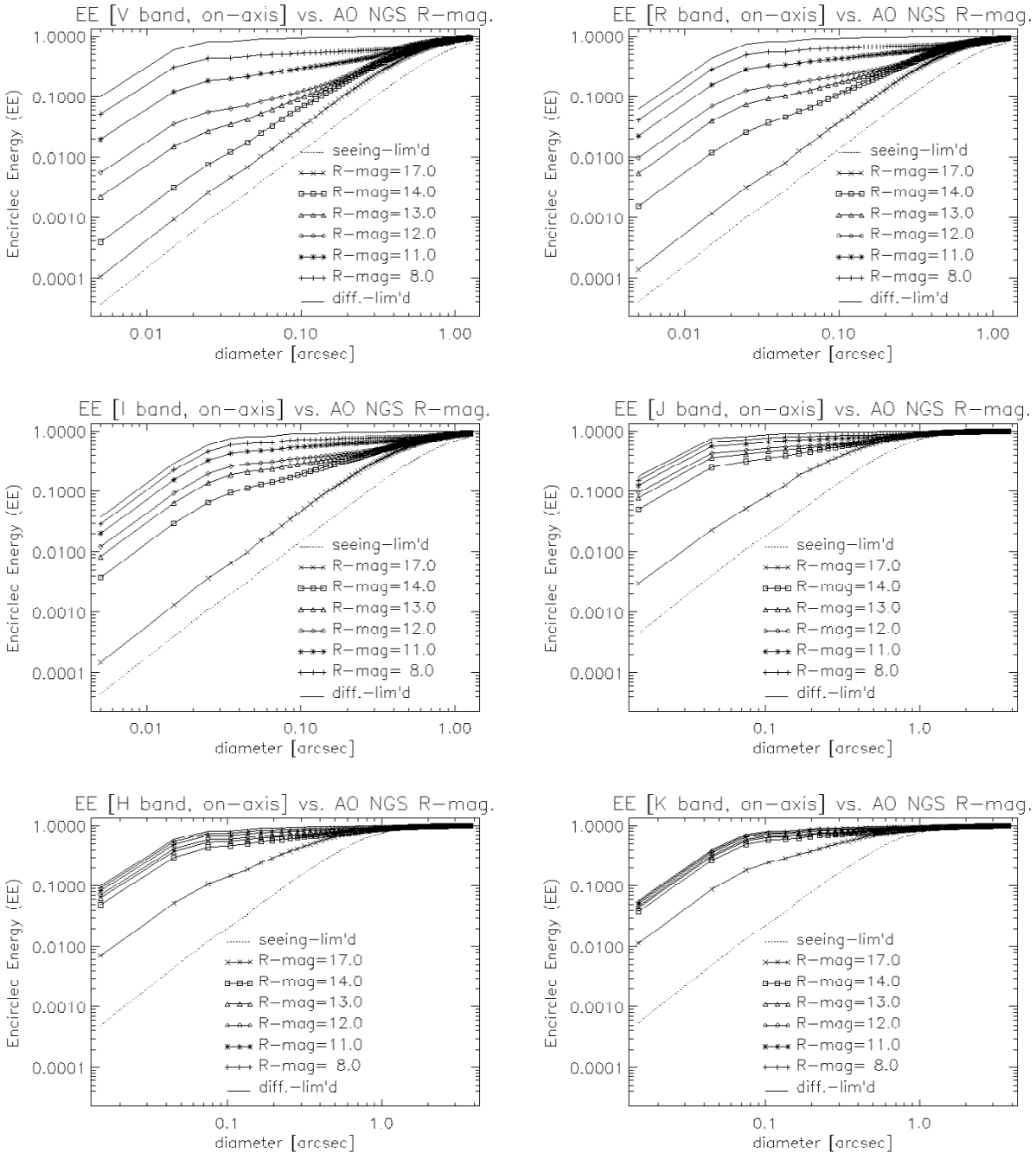

Figure 4. On-axis encircled energy in function of the observing band and the AO guide star R-magnitude. From top to bottom and from left to right: V band, R band, I band, J band, H band, K band.

and where Δt is the time exposure, ρ represents the weight due to the corrected AO-guide-star image morphology (which is consequently strongly dependent upon the off-axis angle), SNR is the signal-to-noise ratio to be attained, $n_{\rm px}$ is the number of pixels under the circular mask (photometric case) or the slit per spectral resolution element (spectroscopic case), $N_{\rm bg}$ is the number of photons per second from the sky background, $N_{\rm d}$ corresponds to the dark current noise contribution, and σ_e is the read-out-noise rms. Concerning $N_{\rm bg}$, the photons coming from the wings of the partially corrected AO guide star are also taken into account into it when considering a very close object observed (typically $0\farcs3$ here).

In Table 5 we have reported the parameters used for the limiting-magnitude calculations presented here.

Table 5. Limiting magnitudes computation parameters.

band	OH fraction	slit width	spectral resolution
J	0.93	$0.075''$	0.033 nm/slit $\Rightarrow \sim$37900
H	0.95	$0.105''$	0.060 nm/slit $\Rightarrow \sim$27500
K	0.50	$0.135''$	0.105 nm/slit $\Rightarrow \sim$21000

In practice, the coupling with the instrument LUCIFER has been studied by taking the output images obtained during the "raw" performance evaluation described in previous section, and performing a series of simulations made by varying the observed object magnitude and computing the resulting limiting magnitude considering the given exposure time and the desired SNR.

Two schemes have been then considered, reported in the following.

Photometric detection

The first scheme considered concerns the photometric detection performance. Basically, we evaluate here until which magnitude an object can be detected with a SNR of 3, a time-exposure of 1800 s, and in function of the angle separating the observed object (a star) from the AO guide-star. The obtained result are shown in Fig. 5.

A remarkable case is the one corresponding to an off-axis angle of $0\farcs3$ for which the limiting magnitude readily drops down. This is due to the morphology of the partial AO corrected image of the AO guide-star itself that is superimposed with the observed object image.

Spectroscopy

The second scheme deals with the spectroscopic performance, where a spectral resolution has been fixed (see Table 5). The result obtained are reported in Fig. 6, in terms of limiting magnitudes and optimal slit length.

5. CONCLUSION

We have reported our latest results concerning the performance evaluation of the first-light AO system of LBT, considering also here the subsequent scientific instrumentation (and especially LUCIFER). The results were given in all bands of interest (V, R, I, J, H, K) in terms of encircled energy, and detailed were given for the near-infrared wavelengths in terms of SNR and limiting magnitudes.

ACKNOWLEDGMENTS

Thanks are due to Christophe Vérinaud for the developments made for the physical modeling of the CAOS module `PYR`, that mimics the pyramid wave-front sensor, and for Bruno Femenía for the developments made for the CAOS module `IMG`, that permits to compute the resulting PSFs and images. Luca Fini is also thanked for the CAOS Application Builder maintaining, and Alfio Puglisi for the intensive computing support.

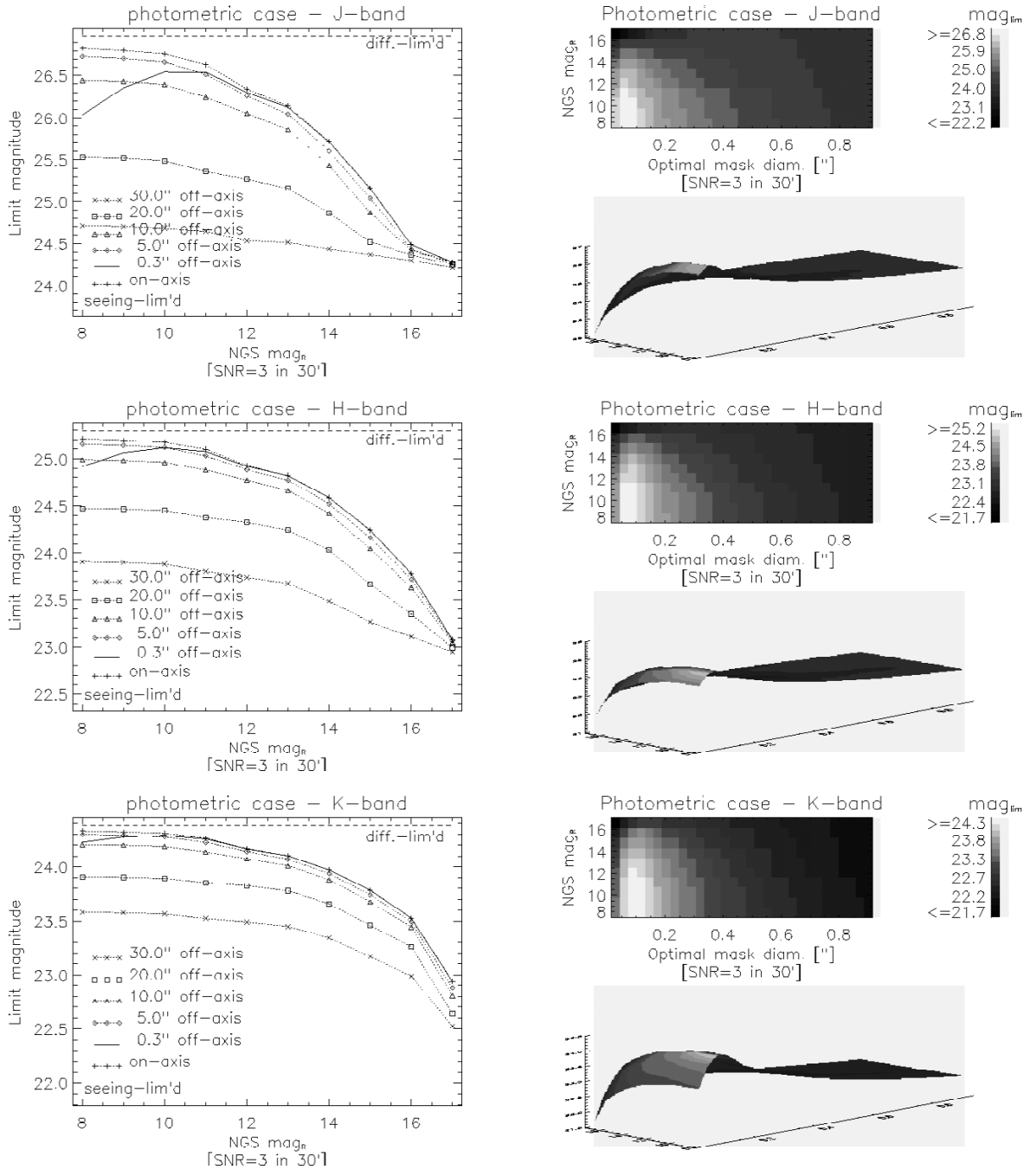

Figure 5. Photometric performance result in the bands J, H, and K, in terms of limiting magnitudes for the various off-axis angles considered (left-part plots), and in terms of optimal mask diameter (right-part plots).

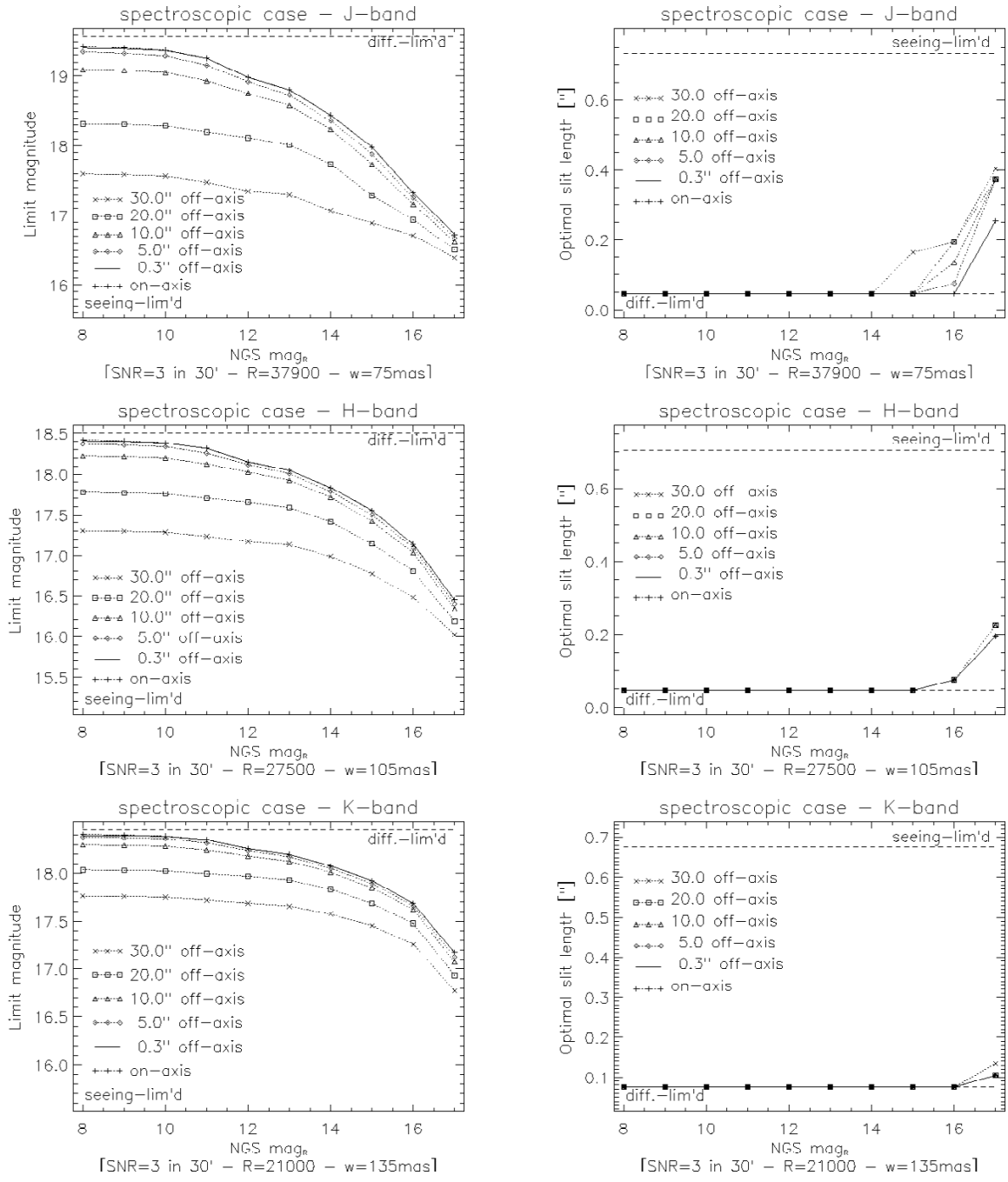

Figure 6. Spectroscopic performance result in the bands J, H, and K, in terms of limiting magnitudes for the various off-axis angles considered (left-part plots), and in terms of optimal slit length (right-part plots).

REFERENCES

1. M. Carbillet, C. Vérinaud, B. Femenía, A. Riccardi, L. Fini, submitted to MNRAS, 2004a.
2. M. Carbillet, C. Vérinaud, M. Guarracino, et al., these proceedings, 2004b.
3. S. Esposito, A. Tozzi, A. Puglisi, et al., these proceedings, 2004.
4. L. Fini, M. Carbillet, A. Riccardi, in *ASP Conf. Ser.* **238**, F. A. Primini & F. R. Harnden Eds, 253, 2001.
5. L. Fini & M. Carbillet, in *ASP Conf. Ser.* **295**, H. E. Payne, R. I. Jedrzejewski, and R. N. Hook Eds., 347, 2003.
6. A. Riccardi, G. Brusa, M. Xompero, et al., these proceedings, 2004.